Eur. J. Mineral.
2019, **31**, 301–312
Published online 9 January 2019

**Mineral reactivity:
from biomineralization and Earth's climate evolution
to CO_2 capture and monument conservation**

Analysis of tempered bricks: from raw material and additives to fired bricks for use in construction and heritage conservation

Natalie SAENZ[1], Eduardo SEBASTIÁN[2] and Giuseppe CULTRONE[2,*]

[1]Department of Chemistry, Columbia University, New York, NY 10027, USA
*Corresponding author, e-mail: cultrone@ugr.es
[2]Departamento de Mineralogía y Petrología, Universidad de Granada, Avenida Fuentenueva, s/n, 18002 Granada, Spain

Abstract: Throughout history, human civilizations have combined clay soils with additives to produce better brick building material. Recently, bricks have been used as a method of eliminating industrial and agricultural wastes by incorporating the waste into brick raw mixtures. In this paper, the effects of three additives on the clay mixture and the fired bricks have been studied. Clayey soil from Jun (Granada, Spain) was combined with fly-ash, household glass and spent beer grain in manually made bricks fired at 800 °C, 950 °C and 1100 °C. Differences in mineral composition, porosity, water behavior, mechanical resistance and color were analyzed through chemical, mineralogical, textural and physical analyses. The presence of carbonates in the clayey soil favored the formation of Ca (–Mg) silicates such as gehlenite, diopside and anorthite in the fired bricks. Only bricks with fly ash displayed growth of secondary acicular calcite crystals. Overall, the additives altered brick porosity and compactness. Bricks made with added glass were found to be the most compact and resistant bricks while those made with spent beer grain were the most porous and fragile. These results have important implications for the construction industry and for the conservation of architectural heritage.

Key-words: solid bricks; fly ash; household glass; spent beer grain; mineralogy; texture; physical properties.

1. Introduction

Though humans have been firing clays since the Neolithic period about 13 000 BCE, the use of bricks in construction developed more slowly (Warren, 1999). The resistance of fired clay to water was a serious advantage over mud-brick, and the technology spread quickly. For a brief review relating the mechanical and thermal properties of archaeological and ethnographic pottery with additives see Tite *et al.* (2001).

Fired bricks are made from clay-rich soils and tend to be extremely porous, though texture and pore shape depend on the firing temperature and the mineral composition of the soil (Hill, 1960; Delbrouck *et al.*, 1993; Cultrone *et al.*, 2004; Karaman *et al.*, 2006). The firing process causes changes in mineral phases and vitrification of the matrix (Orts *et al.*, 1993; Papargyris *et al.*, 2001). These changes at high temperatures give bricks their characteristic hardness and strength (Karaman *et al.*, 2006; Johari *et al.*, 2010; Fabbri, 2012). In addition to firing temperature, brick texture is also heavily dependent on the raw mixture and the method of production (Dondi *et al.*, 1999a; Sveda, 2000; Freyburg & Schwarz, 2007; Murmu & Patel, 2018). Color can depend on the iron content, the presence of impurities and the firing atmosphere (Kreimeyer, 1987; Hendry, 2001; Fabbri, 2012).

Although some brick structures can survive without restoration for thousands of years, others deteriorate very quickly. This depends largely on the quality of the brick (Binda & Baronio, 1984; Robinson, 1984). Because clay soil is produced by rock erosion, transport and sedimentation, it lacks homogeneity, and thus different clays vary in plasticity, workability and shrinkage upon drying. Producing good bricks requires expert knowledge of clay soil composition, tempering agents, production methods, firing temperature, and oven technology (Singer & Singer, 1963; Carretero *et al.*, 2002). For example, calcareous clay works just as well as non-calcareous clay but the manufacturer must be aware of the simple procedures required to prevent lime-blowing, which causes cracks in the bricks after firing (Laird & Worcester, 1956). From a chemical point of view, bricks are practically inert to dissolution processes because they are silicate materials (Warren, 1999). In the presence of water, in liquid or vapor state, the main problem comes from carbonates such as calcite, which is a very common mineral in the clayey soils used as raw materials for brick-making. After firing, any calcite grains that have not reacted with silicates to form new mineral phases turn into lime (CaO). This is a very reactive oxide and when brick is exposed to humidity, the lime reacts with the water forming portlandite ($Ca(OH)_2$). The increase in volume caused by this phase change and by the subsequent carbonation of portlandite into calcite cause the bricks to crack (Laird & Worcester, 1956; Elert *et al.*, 2003).

Brick production today generates huge amounts of waste from quarrying, which also destroys landscapes, and from

https://doi.org/10.1127/ejm/2019/0031-2832

0935-1221/19/0031-2832 $ 5.40

firing, which consumes energy and can release greenhouse gases (Ahmari & Zhang, 2012). These factors explain the increasing interest in making brick production more environmentally friendly (Coletti *et al.*, 2016). The use of waste products as additives can reduce the need for quarrying and solve another environmental problem, the accumulation of industrial and agricultural wastes (Bories *et al.*, 2014). Bricks are ideal because they require the same high firing temperatures many wastes need for safe disposal. Over the last 20 years, several reviews (Dondi *et al.*, 1997; Raut *et al.*, 2011; Zhang, 2013, Muñoz Velasco *et al.*, 2014) have analyzed the use of different toxic waste, sludge, quarry/metallic dust (Shakir *et al.*, 2013), fly ash (Eliche Quesada *et al.*, 2017), and organic wastes in the manufacture of new bricks. The ultimate goal in this line of research would be to incorporate substantial amounts of otherwise burdensome waste products into bricks to make them harder and more porous. Ideally, additives could also improve raw mixture plasticity, reducing the amount of water needed, or increase local temperatures within the brick, so reducing the firing temperature required for vitrification (Muñoz Velasco *et al.*, 2014).

The purpose of this study is to analyze the influences of certain tempering agents on brick characteristics. This study quantifies the impact of additives on the clay mixture and the mineralogical and physical transformations brought about by firing, such as changes in mineral phases, the degree of vitrification, mechanical resistance, water behavior and color change. In addition to solving an environmental problem, these results can enable bricks with specific characteristics to be used in new constructions and in restoration work.

2. Materials and methods

2.1. Materials and additives

The bricks were made out of a clayey soil quarried in Jun (Granada, Spain). Geologically, Jun is situated on the contact limit between the Internal and External Zones of the Granada Basin. The Granada Basin occupies the central portion of the Baetic Cordillera. The area contains Pliocene lacustrine sediments and continental sands and conglomerates deposited over Miocene formations characterized by grayish sediments made up of lime, sands and gravel (Günster & Skowronek, 2001; Vera, 2004). The gray soil was sieved to remove centimetric rock grains, especially gypsum. Large clumps of clay were manually broken up and ground.

Three types of additives were selected for addition to the raw material: fly ash, household glass and spent beer grain. They represent common types of industrial, domestic and agricultural waste products. Fly ash was obtained from a thermoelectric plant in Cadiz (Spain). Fly ash is the finest fraction of ash produced by coal combustion. It is removed from the gases emitted through an electrostatic precipitation process (Eliche Quesada *et al.*, 2017). Most studies of fly ash have focused on its addition to cement and mortars. Previous research into the use of fly ash as an additive in bricks has had mixed results, especially regarding brick strength (Lingling *et al.*, 2005; Fernández-Pereira *et al.*, 2011; Shakir *et al.*, 2013; Abbas *et al.*, 2017). The fly ash used in our research was a soft, dark gray powder with a small amount of white powder clumps. Common household glass jars were broken and ground into powder using an iron mortar. Little research has so far been done on the use of recyclable household glass as an additive in brick production. Lin (2007), Phonphuak *et al.* (2016), Jimenez Millan *et al.* (2018) and Kazmi *et al.* (2018) have demonstrated that bricks with waste glass had enhanced physical–mechanical properties. Spent beer grain was obtained from a Granada beer factory (Spain). This type of residue, also known as bagasse, requires the addition of vitamins when it is recycled as animal feed, soil or fertilizer. Studies with similar waste products such as wheat-straw, corn cob, olive mill solid waste, rice husk, and sugarcane bagasse have all been shown to increase the porosity of bricks (Bories *et al.*, 2014, 2015). Though these additives appear to have similar effects on the resulting bricks, Bories *et al.* (2015) make clear that the expected mineral content, shrinkage, porosity and water absorption should not be overgeneralized to all types of organic wastes. The spent beer grain was dried, manually broken apart and sifted to obtain powder and fibers of less than 1.5 mm. Ideally, if the objective is to use brick production as a means of eliminating waste, the bricks should have a high percentage of added waste. All three additives were dosed at a 20 wt%, a value chosen for comparison purposes because this was the average amount used in previous research (Bories *et al.*, 2014), and also because 20 wt% was a sufficiently high concentration to make changes in the physical characteristics of the bricks more obvious.

2.2. Preparation of the mixture and firing

The raw mixture was prepared by mixing clay soil and the additives, both measured by weight. Although measuring the amount of additive as a percentage of the weight of the mixture facilitates comparison with the literature (Zhang, 2013; Murmu & Patel, 2018), it made comparison of the different additives studied in this paper more difficult. For fly ash and glass additions, there were only minimal differences between weight percent and volume percent added. However, calculating the addition of spent beer grain by weight resulted in adding a volume of grain that was twice that of the clay soil. Water was added after obtaining a homogenous dry mixture which was then mixed by hand until the clay was sufficiently plastic to be put into a wooden mold (4 × 18 × 13 cm). The raw mixture was pressed down firmly by hand into the interior of the mold to cover the bottom, and the rest of the mixture was added with similar force until the mold was filled. The top was scraped to obtain a smooth surface. The raw mixture was allowed to dry within the mold for approximately one hour before the mold was removed. A cotton thread was used to slice the unfired brick into smaller cubes of approximately 4 cm each side and into rectangular prisms of 4 × 1 × 10 cm. The cubes and prisms were separated from one another after

one day of drying to prevent deformation. Before drying was complete, some of the samples were smoothed with a file to remove rough edges. Twelve types of bricks were tested: they were labeled as BN, BA, BG and BS to distinguish bricks with no additives from those with fly ash, household glass and spent beer grain, respectively. Each of these labels is followed by the numbers 8, 9 or 1 in reference to the temperatures at which we decided to fire the bricks: 800 °C, 950 °C and 1100 °C. Bricks factories normally fire at approximately 950 °C. The other temperatures were chosen to enable us to study the mineralogical and physical evolution of the bricks over a range of 300 °C. Firing was carried out in oxidizing conditions in a Herotec CR-35 electric oven. Unfired bricks were placed inside the oven without touching the sides or other bricks. The temperature was first set to 100 °C to rid the bricks of any residual dampness which might cause them to crack due to rapid evaporation. After one hour, the temperature was increased from 100 °C to 400 °C at a rate of approximately 30 °C/min. From 400 °C onwards, the temperature was increased more slowly at approximately 5 °C/min until the desired firing temperature was reached. The oven was then turned off. After firing, bricks were immersed in water for over half an hour to prevent cracking from lime-blowing in case carbonates were present (Laird & Worcester, 1956).

2.3. Analytical techniques

The chemistry of the raw material, the fly ash and the fired samples was studied using X-ray fluorescence. A Philips Magix Pro PW-2440 spectrometer with an ultrafine Rh anode and a 4 kV X-ray generator was used to analyze major and trace elements. Prior to the analysis, 5 g per sample was ground into powder. The accuracy of analytical results was evaluated by comparison with certified values for analyzed reference materials (Govindaraju, 1994). Typical accuracy is higher than 1.5% relative to a concentration of 10%. Loss on ignition was determined gravimetrically as the weight loss was recorded between 110 °C and 1000 °C. The De Jongh model (1973) was followed to convert the intensities into concentrations using Alpha-coefficients.

The identification of the mineral phases in the raw material and the fired bricks with and without additives was carried out by powder X-ray diffraction (PXRD). Samples were analyzed by a Philips X'Pert PRO diffractometer with Cu$K\alpha$ radiation (λ = 1.5405 Å), 45 kV voltage, 40 mA current, 3–60° 2θ explored area and 0.1° 2θ s^{-1} goniometer speed. The interpretation of results was performed using the XPowderX computer program (Martin, 2016). Quantitative analysis of the mineral phases was performed using the non-linear least square method to fit full-profile diffractograms and the results were compared with standard values in the database. The Deradifdata database (University of Arizona) (http://www.geo.arizona.edu/~downs/xtal/InXitu/Deradifdata.txt) and the Pattern Intensity Ratio (PIR) factor method were used to identify and quantify the mineral phases and to obtain the amorphous *versus* crystalline phases (a/c) ratio. This ratio is based on the mean value of the intensities, standard deviation and area of the crystal reflection (Martin, 2016).

A FEI high-resolution environmental scanning electron microscope (FEG-ESEM) with QUEMSCAN 650F operated at 5 kV was used to analyze carbon-coated brick fragments. Energy dispersive X-ray (EDX) analysis was used for elemental analysis of crystals within the fragments.

A detailed mineralogical study was performed by means of a transmission electron microscope (TEM) Philips CM20 operating at 200 kV and equipped with an EDAX solid-state energy-dispersive X-ray detector. Powder samples were deposited on carbon-coated Cu grids. Quantitative chemical analyses were obtained in STEM mode using a scan window of 20 × 100 nm. Muscovite, albite, biotite, spessartine, olivine and titanite standards were used to obtain *k*-factors for the transformation of intensity ratios to concentration ratios according to Cliff & Lorimer (1975).

Physical assays with water were performed using three bricks from each sample group under controlled temperature and hygrometric conditions (22 °C and relative humidity of 35%). Free and forced water absorption (UNE-EN 13755, 2008), drying (NORMAL 29/88, 1988) and capillarity tests (UNE-EN 1925, 2000) were carried out, enabling us to ascertain the degree of pore interconnection (Cultrone *et al.*, 2003), the drying index, the saturation coefficient, apparent and real densities, the open porosity and the capillary coefficient (RILEM, 1980). Cubic samples were used for absorption-drying tests and prism-shaped samples for the capillarity test.

The compactness of the bricks was measured using a Control 58-E4800 ultrasonic pulse velocity tester with 54 kHz transducers and a contact surface of 3 cm in diameter. A viscoelastic gel was used to obtain a good coupling between the transducers and brick surfaces. The speed of P waves was measured on three bricks from each sample group. The transmission method was used in accordance with the ASTM D2845 standard (2005) on dry cubic samples in three orthogonal directions: V_{P1} is the velocity perpendicular to the compaction plane of the raw material in the wooden box and V_{P2} and V_{P3} are the velocities parallel to it. The total and relative anisotropies (ΔM and Δm, Guydader & Denis, 1986) were also calculated.

A SINT Technology DRMS (Drilling Resistance Measurement System) Cordless was used to measure brick resistance by microdrilling. The drill (5 mm in diameter, with flat diamond head) was set to bore 10 mm at 300 r/min with a penetration speed of 20 mm/min. Samples from each group were drilled a minimum of three times for each face.

Finally, the color of the bricks was measured by spectrophotometry in accordance with the UNE-EN 15886 standard (2011) in order to quantify any changes produced by additives or firing temperatures. A Konica-Minolta CM-700d spectrophotometer was used for this purpose and the results were analyzed with SpectraMagic NX software. The working conditions were: circular measurement area of 8 mm diameter, D65 illuminant, 10° vision angle, SCI/SCE mode and light radiation range between 400 nm and 700 nm. The CIELab space color was used.

Three measurements per brick type were performed. To compare the color of the samples with additives to those without additives, the color difference (ΔE) was determined according to the following equation:

$$E = \sqrt{\left(L_1^* - L_2^*\right)^2 + \left(a_1^* - a_2^*\right)^2 + \left(b_1^* - b_2^*\right)^2}, \quad (1)$$

where L_1^*, a_1^*, b_1^* are the lightness and chromaticity values for the bricks without additives and L_2^*, a_2^*, b_2^* are those for bricks with additives.

3. Results

3.1. Macroscopic observations of unfired and fired bricks

The mixture with fly-ash was very sticky, as was the clayey soil with no additives. The addition of fly ash resulted in a very dense mixture with fairly good plasticity, which decreased the workability. Linear drying shrinkage was between 3% and 6%. Because the spent beer grain was very light (and added by wt%) and the fibers readily absorbed water, a comparatively larger volume of water was needed for mixing. The grain fibers made slicing the clay mixture with thread more difficult. Linear drying shrinkage was approximately 2%. Some of the glass was not fully powdered which made the raw material rougher. The mixture with glass was very dense though not overly difficult to work with. Tiny reflective bits of glass could be seen in the unfired bricks. Linear drying shrinkage for bricks with glass was between 2% and 6%.

Fired bricks were distinguishable by the change in color from gray to pink-red and almost yellow. When soaked in water, a small amount of precipitate was released which was later identified with PXRD as calcite. The expansion due to firing was minimal, approximately 1% for most samples. Bricks tempered with fly ash (BA) and fired at 800 °C and 950 °C were covered on all faces by a thin light-gray layer identified by PXRD as calcite. The spent grain within the bricks burnt away as could be verified both by the smell emitted from the oven during firing and visually by the holes left in the bricks (BS). The surfaces of the spent grain bricks turned out to be very delicate and in particular those fired at lower temperature, which suffered a loss of material when picked up. In the bricks made with added glass (BG), the larger bits of glass visible in the mixture remained visible after firing.

All the bricks, especially those made with spent-grain (BS), were noticeably lighter after firing. Figure 1 shows the percentage weight loss of the bricks after firing. The spent-grain bricks lost much more weight than any other type of brick because of the burnt organic matter. Regardless of their firing temperature, the bricks with spent grain lost approximately 21–22% of their initial mass. The bricks made with ash (BA) or glass (BG) lost less weight than the bricks without any additives (BN). Weight loss in these bricks is due to the decomposition of carbonates and the dehydroxylation of phyllosilicates, minerals that appear in smaller quantities in the bricks containing fly ash or glass.

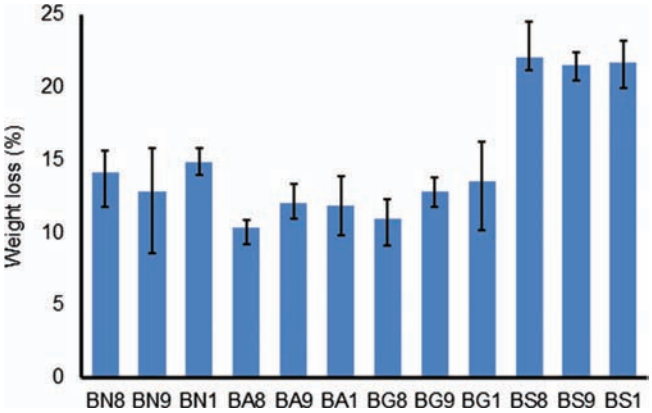

Fig. 1. Average weight loss (in %) of bricks without additives (BN) and with added fly ash (BA), household glass (BG) and spent beer grain (BG) after firing. Error bars indicate maximum and minimum values.

The additives had a greater impact on weight loss than the firing temperature, since higher firing temperatures did not always result in greater weight loss.

3.2. Chemistry and mineralogy of bricks

Bulk chemical analysis of clay soil, fly ash and fired samples shows that the major compound present is SiO_2 followed by Al_2O_3 (Table 1). The presence of CaO in amounts greater than 6% means that the clay soil can be classified as calcareous (Tite *et al.*, 2001). The fly ash is very similar in chemical terms to the clay soil, which is why the fly ash bricks (BA) have a similar mineral composition to those made without additives. The bricks made with glass have slightly lower percentages of Al_2O_3 and higher percentages of Na_2O. The chemical analysis of trace elements shows that the fly ash has many more trace metals, which explain why the bricks made with fly ash have a higher metal content. In this sense, the bricks made with glass or spent beer grain are more similar to the bricks without additives.

The PXRD analysis reveals that the clay soil is rich in quartz and also contains gypsum, calcite and lesser amounts of dolomite, both alkali feldspar and plagioclase, and phyllosilicates. The phyllosilicates are composed of illite/muscovite, chlorite and paragonite. Many of these minerals underwent pyrometamorphism during the firing process.

Overall, the additives did not have a huge influence on the mineral phase changes, as the percentages of each mineral did not vary significantly between samples with different additives fired at the same temperature (Table 2). Quartz is the most common mineral phase. Its concentration decreases as the firing temperature increases because the grain boundaries of this tectosilicate react to form new mineral phases. It has been demonstrated that this reduction is usually more pronounced in bricks made with carbonate-rich soils (Dondi *et al.*, 1999b; El Ouahabi *et al.*, 2015). For bricks fired at 800 °C and 950 °C, quartz continues to be the most common mineral. For samples fired at 1100 °C, anorthite and diopside are just as or more abundant than quartz (Table 2). Chlorite and paragonite disappear completely with

Table 1. X-ray fluorescence bulk chemical analysis of clay soil, fly-ash, and fired brick samples without additives (BN), and with added fly ash (BA), glass (BG) and spent beer grain (BS) fired at 800 °C (8), 950 °C (9) and 1100 °C (1). Major elements are expressed in percentages (%), trace elements in ppm. LOI is the percent weight lost on ignition. Data are normalized to 100% (LOI free).

	Clay soil	Fly ash	BN8	BN9	BN1	BA8	BA9	BA1	BG8	BG9	BG1	BS8	BS9	BS1
SiO_2	50.66	57.23	48.77	48.76	48.26	50.56	49.29	49.60	50.83	50.20	56.31	47.62	46.96	47.33
Al_2O_3	20.62	20.27	19.43	18.89	18.60	20.17	19.46	19.54	18.29	17.34	13.08	19.28	18.67	18.99
Fe_2O_3	6.29	7.26	6.47	6.57	6.66	6.55	6.70	6.77	5.92	5.83	5.65	6.46	6.58	6.67
MnO	0.08	0.07	0.09	0.10	0.10	0.09	0.08	0.09	0.08	0.09	0.08	0.10	0.09	0.10
MgO	4.31	1.51	5.63	6.01	6.55	4.53	5.56	5.71	5.06	5.90	4.60	5.87	6.44	6.40
CaO	13.01	9.24	14.79	14.86	15.22	13.33	14.37	13.91	14.32	14.81	13.94	15.09	15.86	15.15
Na_2O	0.81	0.96	0.64	0.73	0.73	0.71	0.74	0.82	1.58	2.59	2.98	0.65	0.74	0.75
K_2O	3.28	2.30	3.27	3.17	2.94	3.13	2.83	2.59	3.06	2.42	2.56	3.29	3.07	2.88
TiO_2	0.85	1.01	0.81	0.82	0.83	0.84	0.86	0.87	0.77	0.74	0.73	0.79	0.79	0.82
P_2O_5	0.09	0.15	0.10	0.10	0.11	0.11	0.11	0.12	0.09	0.09	0.07	0.85	0.78	0.91
V	152.2	306.8	144.8	145.6	134.1	156.6	162.6	149.6	187.1	189.4	192.2	157.1	162.4	162.5
Cr	83.4	113.5	76.2	78.3	79.4	78.4	79.9	84.8	87.7	89.6	91.1	80.8	84.3	84.4
Co	20.0	25.3	17.9	21.0	10.5	20.2	17.2	21.6	24.6	14.2	22.2	16.4	25.7	18.6
Ni	39.3	63.0	35.9	36.9	37.1	43.8	44.3	44.1	47.7	49.3	50.1	42.2	44.6	46.1
Cu	20.1	54.9	21.5	19.4	21.2	25.8	25.7	26.7	34.2	33.7	33.6	31.0	33.6	32.1
Zn	74.5	150.7	69.7	71.2	71.5	83.8	84.7	84.2	100.4	104.6	103.2	98.5	97.4	76.3
Ga	16.0	19.1	14.9	15.1	14.8	18.7	18.5	18.5	18.7	19.2	19.1	17.9	18.4	19.1
As	22.4	26.6	19.4	20.8	21.5	25.3	23.7	24.9	25.3	26.8	25.5	23.5	26.0	12.2
Cd	0.3	0.6	0.6	0.7	0.8	0.8	0.9	0.8	0.7	1.0	0.9	0.8	0.9	1.0
Zr	172.6	187.0	190.9	205.1	208.5	194.1	212.8	208.7	171.6	186.9	187.5	188.5	203.7	206.1
Nb	13.4	12.7	11.8	12.2	12.4	15.6	15.6	16.0	15.4	16.0	15.6	15.1	16.0	16.1
Mo	1.5	8.1	1.3	1.4	1.5	1.8	1.6	1.9	3.0	3.2	3.0	2.0	2.3	1.8
Ba	409.5	703.8	406.5	415.6	425.3	436.3	467.1	438.4	484.1	530.1	518.9	422.8	453.8	475.3
Pb	16.6	22.7	18.5	18.1	18.4	19.2	20.2	19.9	20.8	22.4	22.0	19.9	11.3	4.7
LOI	14.30	5.14	4.54	1.43	0.34	3.81	1.03	0.13	5.07	0.75	0.16	5.84	0.50	0.08

Table 2. Mineralogical composition by PXRD of the brick samples with and without additives. Qtz = quartz (789), Ill/Ms = illite/muscovite (2013), Cal = calcite (98), Dol = dolomite (86), Anh = anhydrite (5117), Hem = hematite (143), Mc = microcline (5216), Or = orthoclase (313), Sa = sanidine (18062), Ab = albite (536), An = anorthite (370), Geh = gehlenite (5090), Di = diopside (1334), a/c = amorphous-crystalline ratio. AMCSD codes are indicated in brackets after each mineral name. Mineral abbreviations after Whitney & Evans (2010).

	BN8	BN9	BN1	BA8	BA9	BA1	BG8	BG9	BG1	BS8	BS9	BS1
Qtz	39.6	35.6	24.0	41.7	37.6	26.3	31.4	36.2	13.1	37.0	36.4	17.2
Ill/Ms	8.8	7.9		10.0	8.0		10.5	6.7		12.9	5.7	
Cal	2.6			3.3			7.4			6.0		
Dol							4.9					
Anh	6.0	6.5	7.1	6.2	4.0	2.6	6.9	9.8	7.0	5.6	6.8	5.0
Hem	1.2	1.5	1.6	1.7	1.9	1.1	1.2	1.6	0.8	1.4	1.6	1.1
Mc	14.8			18.8			8.8			15.1		
Or	17.6	11.4			7.5		18.3	11.2		11.1	5.9	
Sa		9.2	7.0		7.0	6.6		7.5	4.7		5.3	8.5
Ab	9.4			10.7			10.5			11.0		
An		21.4	40.8		24.5	47.2		24.3	45.8		26.5	50.0
Geh		6.5	11.0		8.7	7.4		10.2	4.3		11.8	6.7
Di			8.6			9.0			24.3			11.5
a/c	0.067	0.073	0.124	0.075	0.095	0.104	0.081	0.100	0.320	0.062	0.091	0.181

firing. The illite/muscovite phase diminishes in concentration with increased firing temperature and is not present at 1100 °C. After firing at 800 °C, dolomite had already disappeared except in the bricks made with glass (BG), probably because of large crystals that did not decompose completely. Calcite remains present, albeit at a lower concentration compared to the clay soil. Above 800 °C, calcium carbonate decomposes into CaO and CO_2 and is not present in bricks fired at 950 °C. Instead, new calcium-rich silicate minerals appear, such as gehlenite ($Ca_2Al_2SiO_7$), which develops from the reaction between calcite and silicates (either illite or K-feldspar) (Cultrone *et al.*, 2001). At 1100 °C, diopside ($CaMgSi_2O_6$) also develops from the reaction between dolomite and quartz (Cultrone *et al.*, 2001). The bricks made

with glass (BG) had larger amounts of diopside than the other groups. Glass seems to enhance a carbonate–silicate reaction. In fact, BG1 has the lowest quartz content (Table 2). Feldspars also undergo transformation upon firing. Potassium feldspars display notable structural changes from microcline (triclinic), present before firing and in bricks fired at 800 °C, to orthoclase (monoclinic), present in bricks fired at 800 °C and 950 °C, and finally to sanidine (monoclinic) present in bricks fired at 950 °C and 1100 °C. Plagioclases also change composition from Na-rich crystals (albite) at 800 °C to a Ca-rich phase (anorthite) at 950 °C and 1100 °C. As mentioned previously, anorthite is the most abundant phase detected by PXRD at 1100 °C. The gypsum present in the clay soil was converted into anhydrite, the dehydrated phase, in the fired bricks. Hematite was detected in all samples. Calcareous clays are known to start to vitrify at lower temperatures than non-calcareous soils since calcite and dolomite act as melting agents (Cultrone *et al.*, 2001; Trindade *et al.*, 2009; Fabbri *et al.*, 2014). Interestingly, in all the samples the ratio between amorphous and crystalline phases increased with higher temperatures, which suggests a gradual increase of matrix vitrification. Bricks with added glass had the highest ratio values (Table 2).

3.3. Texture

Secondary-electron ESEM images show the morphology of the bricks at the microscopic level, the degree of vitrification, and the development of new mineral phases. The presence of (or reliefs from in the case of spent beer grain) additives can clearly be recognized in the samples. In general, lower temperature samples have rougher surfaces with many small laminar sheets of clay. These phyllosilicate sheets fuse at higher temperatures, which means that the bricks fired at 950 °C and 1100 °C have smoother, glassier textures and show the development of new crystal phases.

Bricks without additives clearly demonstrate the process of phyllosilicate melting and vitrification. BN8 and BN9 contain small spherical particles (Fig. 2a) which, when analyzed by EDX, were identified as Mg. These particles probably resulted from decomposed dolomite grains. These bricks also contain phyllosilicate laminae that have fanned out from their original stacked formation due to the heat. The formation of secondary porosity by bubbles of escaping gases can clearly be seen in BN1 (Fig. 2b). In the top left-hand corner of this image we can see melted phyllosilicates, a common occurrence in the samples fired at 950 °C and 1100 °C.

In the samples made with fly ash (BA), the ash particles appear as spheres that vary in size from approximately 1 to 10 μm in diameter. In bricks fired at 800 °C and 950 °C, fly ash spheres and elongated crystals with prismatic trigonal habits are interspersed throughout the clay matrix (Fig. 2c). At 950 °C these crystals show an irregular morphology with rougher surfaces still maintaining a strong development along their ternary axis (Fig. 3a). The ESEM-EDX analysis was unable to define the chemical composition of these crystals due to their size. These crystals are no longer present in bricks fired at 1100 °C (Fig. 2d) and the clay matrix has fused with the spheres. BA was the only brick group in which these acicular crystals appeared, which means that fly ash was involved in their formation. TEM-AEM was implemented to identify the mineralogy and composition of these crystals and explain their formation. Figure 3b shows two acicular crystals of about 500 nm observed under the TEM. The AEM analysis indicates that these crystals are calcium-rich (Fig. 3c) and electron diffraction demonstrates that they are calcite (Fig. 3d). The ESEM images showed that these crystals grew with their *c*-axis normal to the (001) basal plane of partially melted phyllosilicate platelets (Fig. 3a, inset). These observations, suggesting an oriented crystallization of calcite onto phyllosilicates, are consistent with the results by Stephens *et al.* (2010), who demonstrated the epitactic growth of calcite on the (001) plane of partially weathered muscovite crystals at ambient humidity. In our case, illite/muscovite crystals are clearly much more damaged since they are dehydroxylated and partially melted, but it is significant that calcite grew on the tetrahedral layers of mica crystals that underwent firing at 800 °C and 950 °C. Considering that calcite decomposition begins around 600 °C and is completed at ~850 °C (Rodriguez Navarro *et al.*, 2009), its formation most likely took place after firing, *i.e.* during cooling or when samples were soaked in water to prevent lime blowing. It is possible that not all Ca present in fly ash was involved in phase reactions (*i.e.*, formation of high-*T* Ca-silicates) since ash spheres appear intact at 800 °C and 950 °C (Fig. 2c). During cooling or, more probably, during water immersion when a large amount of water comes into contact with the bricks, it seems that the Ca present either as CaO or $Ca(OH)_2$ is released, so enabling the growth of calcite as acicular crystals. In fact, we observed a rapid increase in pH from 7.87 to 9.70 when fly ash was added to the kneading water. The irregular morphology with rough surfaces of calcite is similar to the dendritic morphology described by Tiller (1991) and suggests that calcite growth took place quickly. At 1100 °C ash spheres lose their smooth morphology and begin to fuse to the matrix. At this temperature, the ions are highly mobile which favors the incorporation of all available Ca in the BA bricks to form new silicates (gehlenite, diopside and, above all, anorthite), thus preventing secondary calcite crystallization after firing. This would also explain why the grayish layer develops at 800 °C and 950 °C but not at 1100 °C.

In the bricks made with glass fired at 800 °C (samples BG8), angular fragments of glass were identified. At 950 °C, the vitrification of the matrix begins as manifested in a melted "dripping" appearance (Fig. 2e). The vitrification provokes the formation of rounded pores with smooth surfaces seen in the samples fired at 1100 °C. The highest temperature spurs the formation of new crystals that grow "frame" first, *i.e.* skeletal-growth (Fig. 2f), which suggests a rapid growth and high degrees of supersaturation. The EDX analysis of these crystals identified a combination of Si, Mg and Ca, which suggests that the crystals are most likely diopside.

The ESEM images of the samples prepared with spent beer grain show how the organic material has been burnt away, leaving enormous pores with the imprint of the beer grain vegetable-like fiber (Fig. 2g). For bricks fired at

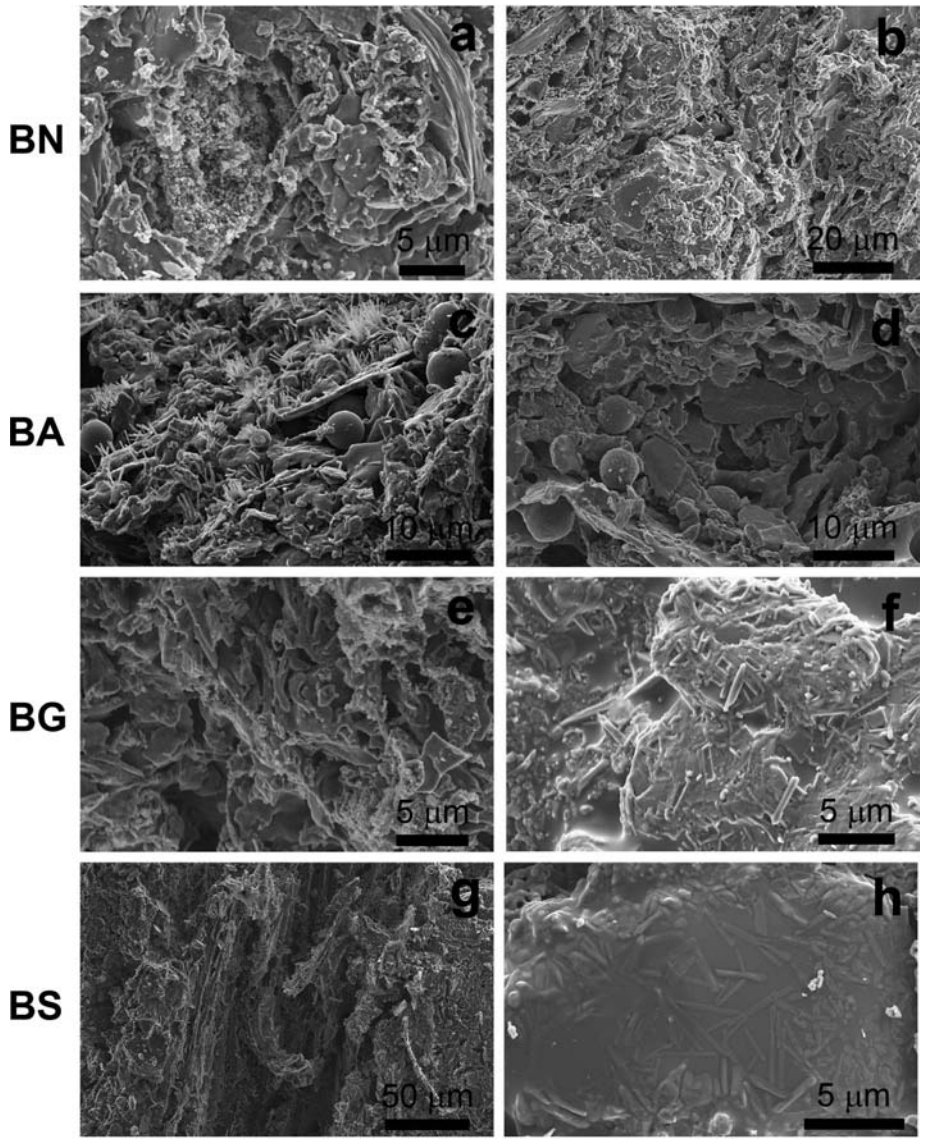

Fig. 2. Secondary-electron ESEM images of bricks with and without additives fired between 800 °C and 1100 °C. (a) BN9 general view with deformed phyllosilicate sheets and decomposition of carbonate grains; (b) BN1 smooth surface and rounded pores from bubbles. A partially-melted phyllosilicate can be seen in the top left-hand corner; (c) BA9 general view with ash spheres and acicular crystals; (d) BA1 brick has a smooth surface and newly formed rounded pores. The matrix fusing to ash spheres with rough surfaces can also be seen; (e) BG9 smooth texture with the presence of secondary pores and melting of the matrix; (f) BG1 close-up of randomly oriented prismatic crystals; (g) BS8 general view of macropore and fiber plant relief; (h) BS1 detail of smooth surface and new mineral formation.

950 °C, macropores with plant reliefs are still visible, but in the bricks fired at 1100 °C the surface is smooth and contains micropores from crystals that have melted together. Moreover, at 1100 °C, the surface shows signs of new prismatic crystal formation (Fig. 2h). The EDX analysis (detection of Si, Mg and Ca) indicates that these crystals are again diopside. In the beer grain bricks, diopside crystals vary in size according to their position. On the inner section of the surface in Fig. 2h, a few large crystals can be seen, while large numbers of small crystals form on the outside. This difference in growth probably depends on the mineral concentrations at the crystal nucleation phase. The smaller crystals on the outside were formed due to the many nucleation points available because of the abundance of ions. The inner section has fewer nucleation sites and larger crystals are formed by ions that slowly seep into and enlarge the crystals.

3.4. Physical tests

Hydric assays are a basic way to measure brick density, porosity and degree of connection, among other standard coefficients shown in Table 3. Bricks without additives present fairly high ranges of water absorption (A_b and A_f, Table 3), absorbing approximately a quarter of their weight in water. The addition of fly ash results in more absorbent

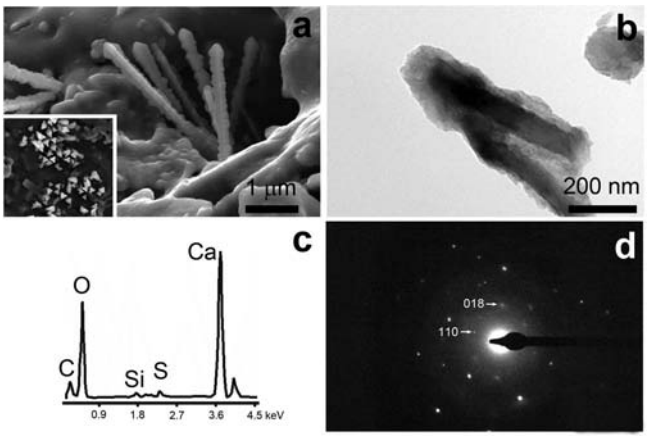

Fig. 3. Detailed observation and analysis of acicular crystals in BA9 brick. (a) close-up of crystals with trigonal morphology observed under ESEM. The inset in the lower left corner shows the *c*-axis of acicular crystals normal to the basal plane of phyllosilicates (the width of image measures 5 µm); (b) TEM image of two crystals; (c) AEM spectrum revealing the elemental composition of these crystals; (d) selected area electron diffraction pattern of [8$\bar{8}$1] zone axis of the calcite crystal in (b).

bricks. The bricks tempered with glass are the least absorbent. The bricks made with spent beer grain (BS) are by far the most absorbent, absorbing about 70–75% of their weight (Table 3). There are no norms establishing maximum of water absorption values, although they rarely exceed 35% (Esbert *et al.*, 1997); BS bricks in our study are well outside this limit.

Figure 4 shows the average free water absorption, forced water absorption and drying of samples of each type of brick. The huge difference in absorption between spent beer grain bricks (BS) and the other samples is immediately noticeable. The spent beer grain bricks also dry quickest as they have the highest drying index (D_i, Table 3). In general, D_i decreases as firing temperatures increase because of the vitrification of the samples (Table 3). Samples with glass (BG) have the lowest drying indices. Bricks release water in two phases. The initial decrease corresponds to the drying of the outer surface area. As the curve flattens out, drying takes place in the core of the brick, and is much slower (Scherer, 1990; Benavente *et al.*, 2007). The saturation coefficient (S, Table 3) is extremely high for all samples except BG1. It tends to decrease slightly as firing temperatures increase. Among the different groups, the samples with spent beer grain have the lowest range of values, between 83% and 86%, even though they have the highest absorption levels. These values mean that spent beer grain bricks were not absorbing according to their full potential. This aspect is better expressed by the interconnectivity constant (A_X) which has the inverse trend (Table 3). Bricks with glass have low interconnectivity which increases at higher firing temperatures. The bricks with glass fired at 1100 °C (BG1) have the lowest number of pore interconnections followed by those with spent beer grain. Thus, not only do bricks made with spent beer grain have more pores, but the connection between them is worse than in the other bricks. The highest capillary coefficient (C_C) in all the samples was for the bricks fired at 950 °C, followed by those fired at 1100 °C and finally those fired at 800 °C. This pattern might be related to the types of pores present. Water can be absorbed by capillarity more effectively when there are many small, interconnected pores. Partial vitrification and incipient secondary pore formation in bricks fired at 950 °C might be such that the water absorption through capillarity reaches a maximum speed. The samples have similar C_C values, although they are highest for bricks without additives. The open porosity of the bricks made with fly ash and spent beer grain was over 40%, the latter reaching values of 62% (P_O, Table 3). The addition of glass decreases P_O to approximately 30%. According to Esbert *et al.* (1997), P_O should not exceed 40%. Clearly, the fact that the bricks were made by hand and contained certain additives (fly ash and, above all, spent beer grain) led to higher values being obtained. Apparent density (ρ_a) is inversely related with open porosity following this trend from greatest to least: BG, BN, BA and BS. The bricks without additives (BN) have the highest real densities (ρ_r, Table 3).

In general, ultrasound velocities increase with increased firing temperature (Table 4). The bricks tempered with spent

Table 3. Hydric parameters of brick samples with and without additives. A_b = free absorption (%), A_f = forced absorption (%), A_x = interconnectivity constant (%), S = saturation coefficient (%), D_i = drying index, C_C = capillary coefficient, ρ_a = apparent density (g cm^{-3}), ρ_r = real density (g cm^{-3}), P_O = open porosity (%).

	A_b	A_f	A_x	S	D_i	C_C	ρ_a	ρ_r	P_O
BN8	23.80	24.28	1.97	96.5	0.42	0.54	1.53	2.44	37.14
BN9	25.08	25.84	2.97	95.6	0.37	2.39	1.50	2.45	38.77
BN1	24.00	26.32	8.79	87.0	0.24	1.16	1.45	2.35	38.18
BA8	33.47	35.04	4.47	95.0	0.38	0.51	1.28	2.33	44.99
BA9	35.19	37.12	5.19	94.1	0.36	1.52	1.27	2.38	46.95
BA1	33.64	37.37	9.98	88.2	0.28	0.99	1.24	2.31	46.33
BG8	19.66	20.24	2.89	95.0	0.34	0.15	1.62	2.42	32.85
BG9	20.52	21.66	5.24	92.7	0.33	2.13	1.57	2.38	34.01
BG1	14.52	20.25	28.28	68.5	0.27	0.80	1.51	2.17	30.53
BS8	69.46	81.90	15.18	83.5	0.39	4.75	0.74	1.89	60.74
BS9	75.83	86.86	12.70	86.8	0.42	1.10	0.72	1.91	62.39
BS1	74.53	86.59	13.93	83.7	0.37	0.93	0.72	1.92	62.50

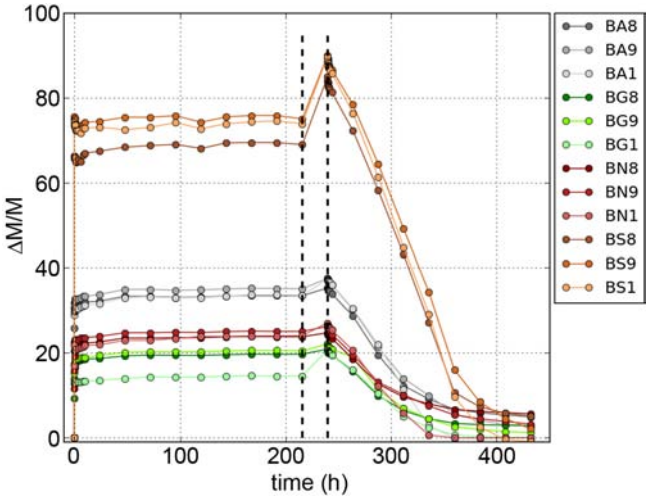

Fig. 4. Water absorption (from *t*0 to *t*240) and drying (from *t*240 to *t*432) of bricks without and with additives by weight variation (Δ*M*/*M*) *versus* time (in hours). The legend on the right matches colors with corresponding samples. The two dotted lines correspond to the period of time during which the bricks were subjected to forced water absorption (under vacuum).

beer grain (BS) have the lowest velocities. The bricks made with glass (BG) or without additives (BN) have higher velocities. This corresponds to BS and BG as the most and the least porous bricks, respectively (P_O, Table 3). Waves going through bricks tempered with glass and fired at the highest temperature (BG1) reach the greatest velocities. The difference in velocities between the three orthogonal sides can be used to determine the anisotropy of the bricks. The main anisotropic character (Δ*M*) compares the velocities between the compaction plane (the bed) and the other two faces (header and stretcher). Δ*M* decreased with increasing firing temperature, which suggests that bricks are reaching more homogenized structures because of vitrification. This value is clearly greater than Δ*m* since this last variable only considers P waves moving perpendicularly to the compaction direction, or in other words, parallel to the oriented phyllosilicates. The greater homogeneity reached by the bricks made with glass fired at 950 °C and 1100 °C produces similar Δ*M* and Δ*m* values.

Microdrilling provides a simple measure of mechanical resistance, a factor related to porosity and hardness. Overall resistance with microdrilling is difficult to quantify because the brick may be very hard where there are larger grains of quartz but also very porous, resulting in highly varying levels of resistance. Table 5 provides mean, standard deviation from the mean and maximum values. These values indicate that the bricks tempered with glass are the most resistant, followed by those with no additives. There is an inverse relationship between these values and those for porosity (P_O, Table 3). On this question, Lu *et al.*, (1999) showed how the increase in porosity of bricks is followed by a substantial decrease in their mechanical properties. Bricks made with fly ash and, above all, those made with spent beer grain are the least resistant. Other than in the glass tempered bricks, firing temperature does not make a

Table 4. Ultrasound average velocities of the three orthogonal brick faces (in m/s) and structural (Δ*M*) and relative (Δ*m*) anisotropies (in %).

	V_{P1}	V_{P2}	V_{P3}	Δ*M*	Δ*m*
BN8	1575	1958	1915	18.63	2.44
BN9	1946	2315	2263	15.00	2.33
BN1	1916	2263	2207	14.22	5.90
BA8	1012	1126	1167	11.59	3.64
BA9	1065	1299	1291	17.78	3.47
BA1	1166	1365	1345	13.98	1.68
BG8	1531	1935	1837	18.49	6.07
BG9	1985	2261	2296	12.80	10.95
BG1	2599	2840	2751	7.04	8.61
BS8	692	961	865	23.30	10.95
BS9	458	763	775	40.42	5.96
BS1	765	1049	1164	30.90	10.94

significant difference on the resistance, although in general the bricks tend to be harder when fired at higher temperatures. In contrast to all the other samples, which underwent small oscillations in drill resistance, the resistance in the samples made with spent beer grain fluctuated dramatically because of the enormous amount of pores. These fluctuations can be deduced from the standard deviations (σ, Table 5). Microdrilling performed in the four brick groups shows the same trend measured by ultrasound: higher mechanical resistance results in higher ultrasonic wave velocity (V_P, Table 4). According to Fernandes & Lourenço (2007), who analyzed historic bricks from several monuments by microdrilling and compared the results with uniaxial compression tests, only BN and BG samples show acceptable resistance values.

Finally, brick color changes were quantified. The influence of the firing temperature on color can be observed by the change in *a** values (Table 6). Brick *a** values decrease with increased firing temperature, which means they lose more of their red component. Furthermore, *L** values tend to increase with firing temperature, making the bricks lighter-colored. All bricks have similar *h*° and *C** values, though the latter are slightly higher in BG and BN. Overall the bricks have very similar colors and tend more towards an orange-pink. In terms of color, the additives cause more significant differences than the firing temperature (Table 6). The bricks without additives (BN) have the highest *a** values, which means that there is a greater "red" component in their color. The decrease in *a** with greater firing temperature is more dramatic in samples with glass and without additives. Bricks with fly ash (BA) and spent beer grain (BS) undergo an increase in *b**, in other words gain in yellow, with higher firing temperatures. The bricks made with fly ash (BA) have higher *L** values because (at least at 800 °C and 950 °C) of the light-gray layer covering the surface. The *L***a***b** values indicate that the samples almost similar in color to those made without additives are the bricks made with glass. The standard deviation between the different samples at each temperature (Table 6) presents a picture of the differences in colors between the faces and the samples at the same temperature. Once again, the bricks made with fly ash

Table 5. Mean values of microdrilling resistance ($\bar{x}$), standard deviations (σ), and maximum values (max) as measured by force (in *N*) measured in brick samples with and without additives.

	BN8	BN9	BN1	BA8	BA9	BA1	BG8	BG9	BG1	BS8	BS9	BS1
$\bar{x}$	14.6	14.8	14.9	3.9	3.1	3.7	19.0	23.4	50.1	1.4	0.7	0.8
σ	8.8	3.1	3.7	1.5	0.7	1.0	6.5	6.3	13.9	0.8	0.4	0.5
max	26.8	19.2	21.6	6.7	4.5	6.5	35.1	38.7	71.6	3.6	1.9	2.4

Table 6. Lightness (L^*), chromatic coordinates (a^* and b^*), chroma (C^*), hue angle ($h°$) for bricks with and without additives. Color difference (ΔE) of the bricks with additives is compared to the bricks without additive fired at the same temperature. Standard deviation from the mean is indicated into brackets.

Sample	L^*	a^*	b^*	C^*	$h°$	ΔE
BN8	58.95 (1.59)	16.80 (1.14)	23.57 (1.51)	28.94 (1.83)	54.53 (0.95)	
BN9	59.81 (2.64)	16.13 (1.70)	21.99 (2.01)	27.27 (2.59)	53.75 (1.03)	
BN1	65.79 (3.12)	10.93 (2.74)	21.37 (1.23)	24.10 (1.98)	63.19 (5.39)	
BA8	66.13 (6.32)	10.09 (5.35)	17.86 (5.41)	20.60 (7.29)	62.26 (6.62)	7.76
BA9	63.96 (9.96)	12.37 (7.88)	19.38 (6.58)	23.20 (9.51)	60.62 (11.71)	4.39
BA1	67.36 (6.08)	9.89 (4.31)	19.94 (2.39)	22.45 (3.66)	64.45 (8.44)	1.58
BG8	56.79 (2.37)	16.83 (1.87)	23.37 (1.87)	28.80 (2.58)	54.32 (1.21)	1.96
BG9	58.08 (1.40)	16.69 (1.45)	22.28 (1.87)	27.84 (2.31)	53.16 (1.07)	1.59
BG1	61.71 (3.51)	8.06 (2.19)	22.14 (1.18)	23.64 (1.52)	70.12 (4.66)	4.40
BS8	60.84 (2.35)	11.83 (3.45)	19.78 (2.46)	23.12 (3.76)	59.69 (4.90)	3.77
BS9	65.36 (1.36)	10.89 (1.21)	21.48 (1.42)	24.10 (1.64)	63.15 (2.09)	6.21
BS1	59.82 (3.94)	10.64 (0.77)	22.96 (1.24)	25.31 (1.40)	65.14 (0.95)	5.16

(BA) display the greatest discrepancy between samples because of the thickness or area of the light-gray layer on the faces of the brick. There was also considerable variation in color amongst the bricks made with glass and fired at 1100 °C and amongst the bricks made with spent beer grain fired at 800 °C. The variations amongst the bricks made with spent beer grain can be observed by a quick glance at the samples, which are characterized by different darker red or orange streaks. Lastly, by calculating the color difference (ΔE), the variation between the different faces and samples can also be shown (Table 6). ΔE values up to 5 refer to color changes that cannot be appreciated by the human eye (Grossi *et al.*, 2007). This limit was only exceeded in three cases. At 800 and 950 °C, glass has the smallest effect on color, while at 1100 °C fly ash bricks are the most similar to those made without additives. Remember that at this temperature secondary acicular calcite crystals no longer exist in BA bricks.

4. Conclusions

This study demonstrates that, in general, the most important differences between the samples were due to the choice or lack of additive. Changing the additive changed the porosity, resulting in differences in density, resistance, water absorption and color. Variations in hardness, vitrification and mineral composition stemmed from differences in the firing temperature. As the temperature rises, carbonates decompose and react with quartz and other silicates to form gehlenite, diopside and anorthite. Alkali feldspars change polymorphs from microcline to sanidine. Phyllosilicates identified in the clay soil had either already disappeared at 800 °C or dehydroxylated and reduced in concentration while the matrix was vitrifying. Secondary acicular calcite crystals only developed in the bricks made with fly ash and only when samples were fired at 800 °C and 950 °C. Their presence is due to the release of Ca from ash particles during the immersion of bricks after firing.

If we compare the changes brought about by the three different additives, we can see the wide range of possible effects that a tempering agent can have on the resulting brick. Although fly-ash and glass appear to have similar effects on raw mixture plasticity, their additions have opposite effects on the finished product. Fly-ash made lighter bricks, increased the porosity and water absorption and decreased the resistance, while the addition of glass decreased the porosity and made the bricks extremely resistant.

The density and porosity values influence the ultrasound and microdrilling resistance results. The ultrasound velocities of bricks fired at higher temperatures are greater because the pores are smaller and the matrix is more unified and vitrified. These characteristics also explain the correlation between higher drilling resistance and higher firing temperature.

The use of spent beer grain radically changed the characteristics of the fired brick. The bricks made with this additive were extremely lightweight, fragile and absorbent, which made obtaining accurate data something of a challenge. By contrast, the bricks made with household glass were very compact and the least absorbent. They also had the lowest porosity and were highly resistant to drilling. Our results therefore indicate that of the additives chosen in this research, the bricks made with household glass are those that

best meet the criteria for use in either conservation or construction.

The combination of mineralogical and physical tests applied during this study has provided new data on how waste products used as additives in brick production can influence the quality of the fired product. These findings relate to various possible options for new and replacement materials of interest for both the brick industry and for those responsible for restoring historical buildings. When bricks of this kind are used in restoration work to replace original brickwork, the aesthetic appearance (*i.e.*, size, color, surface finish) are of crucial importance. The use of bricks made with waste product additives is not *a priori* harmful for old buildings provided that the aesthetics and physical–mechanical properties are similar to those of the original bricks, and the reuse of these waste products is beneficial for the environment. Though promising results have been obtained, future experiments with different concentrations of additives would provide useful complementary information. For example, the low resistance of bricks made with spent beer grain indicates that 20 wt% is too high for making viable bricks. Moreover, potential problems associated with the possible leaching of toxic elements (*i.e.*, present in fly ash) and/or additional potential drawbacks associated with the use of waste material in brick making should require further research and testing prior to the widespread use of these bricks in construction and monument conservation. Finally, exploring other methods of brick production (*i.e.*, preparing the unfired samples by extrusion) would have more industrial applications since the method applied in this study has more in common with traditional methods than with those used in modern brick factories.

Acknowledgements: This study was funded by Junta de Andalucía Research Group RNM179 and by Research Project MAT2016-75889-R. We thank Cerámica Castillo Siles (Granada) for providing the raw material used to prepare and fire the bricks, Cervezas Alhambra S.L. (Granada) for providing the spent beer grain and Los Barrios thermoelectric plant (Cadiz) for providing the fly ash. We are grateful to K. Elert and C. Rodríguez Navarro for their valuable assistance in TEM study. The paper also benefited from the helpful suggestions and comments of two anonymous reviewers.

References

Abbas, S., Saleem, M.A., Kazmi, S.M.S., Munir, M.J. (2017): Production of sustainable clay bricks using waste fly ash: mechanical and durability properties. *J. Build. Eng.*, **14**, 7–14.

Ahmari, S. & Zhang, L. (2012): Production of eco-friendly bricks from copper mine tailings through geopolymerization. *Constr. Build. Mater.*, **29**, 323–331.

ASTM D2845 (2005): Standard test method for laboratory determination of pulse velocities and ultrasonic elastic constant of rock. ASTM, USA.

Benavente, D., Linares-Fernández, L., Cultrone, G., Sebastián, E. (2007): Influence of microstructure on the resistance to salt crystallisation damage in brick. *Mater. Struct.*, **39**, 105–113.

Binda, L. & Baronio, G. (1984): Measurement of the resistance to deterioration of old and new bricks by means of accelerated aging tests. *Durability Build Mater.*, **2**, 139–154.

Bories, C., Borredon, M.E., Vedrenne, E., Vilarem, G. (2014): Development of eco-friendly porous fired clay bricks using pore-forming agents: a review. *J. Environ. Manag.*, **143**, 186–196.

Bories, C., Aouba, L., Vedrenne, E., Vilarem, G. (2015): Fired clay bricks using agricultural biomass wastes: study and characterization. *Constr. Build. Mater.*, **91**, 158–163.

Carretero, M.I., Dondi, M., Fabbri, B., Raimondo, M. (2002): The influence of shaping and firing technology on ceramic properties of calcareous and non-calcareous illitic-chloritic clays. *Appl. Clay Sci.*, **20**, 301–306.

Cliff, G. & Lorimer, G.W. (1975): The quantitative analysis of thin specimens. *J. Microsc.*, **103**, 203–207.

Coletti, C., Cultrone, G., Maritan, L., Mazzoli, C (2016): How to face the new industrial challenge of compatible, sustainable brick production: study of various types of commercially available bricks. *Appl. Clay Sci.*, **124–125**, 219–226.

Cultrone, G., de la Torre, M.J., Sebastián, E., Cazalla, O. (2003): Evaluation of bricks durability using destructive and non-destructive methods (DT and NDT). *Mater. Construct.*, **53**, 41–59.

Cultrone, G., Rodriguez-Navarro, C., Sebastian, E., Cazalla, O., de La Torre, M.J. (2001): Carbonate and silicate phase reactions during ceramic firing. *Eur. J. Mineral.*, **13**, 621–634.

Cultrone, G., Sebastián, E., Elert, K., de la Torre, M.J., Cazalla, O., Rodriguez Navarro, C. (2004): Influence of mineralogy and firing temperature on the porosity of bricks. *J. Eur. Ceram. Soc.*, **24**, 547–564.

De Jongh, W.K. (1973): X-ray fluorescence analysis applying theoretical matrix corrections. Stainless steel. *X-Ray Spectrom.*, **2**, 151–158.

Delbrouck, O., Janssen, J., Ottenburgs, R., Van Oyen, P., Viaene, W. (1993): Evolution of porosity in extruded stoneware as a function of firing temperature. *Appl. Clay Sci.*, **7**, 187–192.

Dondi, M., Marsigli, M., Fabbri, B. (1997): Recycling of industrial and urban wastes in brick production – a review. *Tile Brick Int.*, **13**, 218–225.

Dondi, M., Marsigli, M., Venturi, I. (1999a): Microstructure and mechanical properties of clay bricks: comparison between fast firing and traditional firing. *Brit. Ceram. Trans.*, **98**, 12–18.

Dondi, M., Guarini, G., Raimondo, M. (1999b): Trends in the formation of crystalline and amorphous phases during the firing of clay bricks. *Tile Brick Int.*, **15**, 176–183.

El Ouahabi, M., Daoudi, L., Hatert, F., Fagel, N. (2015): Modified mineral phases during clay ceramic firing. *Clay Clay Minerals*, **63**, 404–413.

Elert, K., Cultrone, G., Rodriguez Navarro, C., Sebastián Pardo, E. (2003): Durability of bricks used in the conservation of historic buildings. Influence of composition and microstructure. *J. Cult. Herit.*, **4**, 91–99.

Eliche Quesada, D., Felipe Sesé, M.A., Moreno Molina, A.J., Franco, F., Infantes Molina, A. (2017): Investigation of using bottom or fly pine-olive pruning ash to produce environmental friendly ceramic materials. *Appl. Clay Sci.*, **135**, 333–346.

Esbert, R.M., Ordaz, J., Alonso, F.J., Montoto, M. (1997): Manual de diagnosis y tratamiento de materiales pétreos y cerámicos. Collegi d'Aparelladors i Arquitectes Tècnics de Barcelona, Spain.

Fabbri, B. (2012): Science and Conservation for Museum Collections. Kermes Quaderni. Nardini Editore, Firenze, Italy.

Fabbri, B., Gualtieri, S., Shoval, S. (2014): The presence of calcite in archaeological ceramics. *J. Eur. Ceram. Soc.*, **34**, 1899–1911.

Fernandes, F. & Lourenço, P.B. (2007): Evaluation of the compressive strength of ancient clay bricks using microdrilling. *J. Mater. Civ. Eng.*, **19**, 791–800.

Fernández-Pereira, C., de la Casa, J.A., Gómez-Barea, A., Arroyo, F., Leiva, C., Luna, Y. (2011): Application of biomass gasification fly ash for brick manufacturing. *Fuel*, **90**, 220–232.

Freyburg, S. & Schwarz, A. (2007): Influence of the clay type on the pore structure of structural ceramics. *J. Eur. Ceram. Soc.*, **27**, 1727–1733.

Govindaraju, K. (1994): Compilation of working values and sample description for 383 geostandards. *Geostandards Newslett.*, **18**, 1–158.

Grossi, C.M., Brimblecombe, P., Esbert, R.M., Alonso, F.J. (2007): Colour changes in architectural limestones from pollution and cleaning. *Colour Res. Appl.*, **32**, 320–331.

Günster, N. & Skowronek, A. (2001): Sediment-soil sequences in the Granada Basin as evidence for long-and short-term climatic changes during the Pliocene and Quaternary in the Western Mediterranean. *Quatern. Int.*, **78**, 17–32.

Guydader, J. & Denis, A. (1986): Propagation des ondes dans les roches, anisotropies sous contrainte, évaluation de la qualité des schistes ardoisiers. *Bull. Eng. Geol.*, **33**, 49–55.

Hendry, H.A.W. (2001): Masonry walls: materials and construction. *Constr. Build. Mater.*, **15**, 323–330.

Hill, R.D. (1960): A study of pore size distribution of fired clay bodies. The effect of clay mineralogy on the distribution. *Trans. Brit. Ceram. Soc.*, **59**, 189–197.

Jimenez Millan, J., Abad, I., Jimenez Espinosa, R., Yebra Rodriguez, A. (2018): Assessment of solar panel waste glass in the manufacture of sepiolite based clay bricks. *Mater. Lett.*, **218**, 346–348.

Johari, I., Said, S., Hisham, B., Bakar, A., Ahmad, Z.A. (2010): Effect of the change of firing temperature on the microstructure and physical properties of clay bricks from Beruas (Malaysia). *Sci. Sinter.*, **42**, 245–254.

Karaman, S., Ersahin, S., Gunal, H. (2006): Firing temperature and firing time influence on mechanical and physical properties of clay bricks. *J. Sci. Ind. Res.*, **65**, 153–159.

Kazmi, S.M.S., Munir, M.J., Wu, J.F., Hanif, A., Patnaikuni, I. (2018): Thermal performance evaluation of eco-friendly bricks incorporating waste glass sludge. *J. Clean. Prod.*, **172**, 1867–1880.

Kreimeyer, R. (1987): Some notes on the firing colour of clay bricks. *Appl. Clay Sci.*, **2**, 175–183.

Laird, R.T. & Worcester, M. (1956): The inhibition of lime blowing. *Trans. Br. Ceram. Soc.*, **55**, 545–563.

Lin, K.L. (2007): The effect of heating temperature of thin film transistor-liquid crystal display (TFT-LCD) optical waste glass as a partial substitute for clay in eco-brick. *J. Clean. Prod.*, **15**, 1755–1759.

Lingling, X., Wei, G., Tao, W., Nanru, Y. (2005): Study on fired bricks with replacing clay by fly ash in high volume ratio. *Constr. Build. Mater.*, **19**, 243–247.

Lu, G., Lu, G.Q., Xiao, Z.M. (1999): Mechanical properties of porous materials. *J. Porous Mat.*, **6**, 359–368.

Martin, J.D. (2016): XPowder, XPowder12, XPowderX^{TM}. A Software Package for Powder X-ray Diffraction Analysis, Lgl. Dp. GR-780-2016.

Muñoz Velasco, P., Morales Ortíz, M.P., Mendívil Giró, M.A., Muñoz Velasco, L. (2014): Fired clay bricks manufactured by adding wastes as sustainable construction material - A review. *Constr. Build. Mater.*, **63**, 97–107.

Murmu, A.L. & Patel, A. (2018): Towards sustainable brick production: an overview. *Constr. Build. Mater.*, **165**, 112–125.

NORMAL 29/88 S. (1988): Misura dell'indice di asciugamento (drying index). CNR-ICR, Rome, Italy,

Orts, M.J., Escardino, A., Amoros, J.L., Negre, F. (1993): Microstructural changes during the firing of stoneware floor tiles. *Appl. Clay Sci.*, **7**, 193–205.

Papargyris, A.D., Cooke, R.G., Papargyri, S.A., Botis, A.I. (2001): The acoustic behaviour of bricks in relation to their mechanical behaviour. *Constr. Build. Mater.*, **15**, 361–369.

Phonphuak, N., Kanyakam, S., Chindaprasirt, P. (2016): Utilization of waste glass to enhance physical-mechanical properties of fired clay bricks. *J. Clean. Prod.*, **112**, 3057–3062.

Raut, S.P., Ralegaonkar, R.V., Mandavgane, S.A. (2011): Development of sustainable construction material using industrial and agricultural solid waste: a review of waste-create bricks. *Constr. Build. Mater.*, **25**, 4037–4042.

RILEM (1980): Recommended test to measure the deterioration of stone and to assess the differences of treatment methods. *Mater. Struct.*, **13**, 175–253.

Robinson, G.C. (1984): The relationship between pore structure and durability of brick. *Ceram. Bull.*, **63**, 295–300.

Rodriguez Navarro, C., Ruiz Agudo, E., Luque, A., Rodriguez Navarro, A.B., Ortega Huertas, M. (2009): Thermal decomposition of calcite: mechanisms of formation and textural evolution of CaO nanocrystals. *Am. Mineral.*, **94**, 578–593.

Scherer, G.W. (1990): Theory of drying. *J. Am. Ceram. Soc.*, **73**, 3–14.

Shakir, A.A., Naganathan, S., Nasharuddin Mustapha, K. (2013): Properties of bricks made using fly ash, quarry dust and billet scale. *Constr. Build. Mater.*, **41**, 131–138.

Singer, F. & Singer, S.S. (1963): Industrial Ceramics. Chapman & Hall, London, UK.

Stephens, C.J., Mouhamad, Y., Meldrum, F.C., Christenson, H.K. (2010): Epitaxy of calcite on mica. *Cryst. Growth Des.*, **10**, 734–738.

Sveda, M. (2000): New look at mathematical relationships among physical properties of brick products. *Brit. Ceram. Trans.*, **99**, 181–186.

Tiller, W.A. (1991): The science of crystallization. macroscopic phenomena and defect generation. Cambridge University Press, Cambridge, UK.

Tite, M.S., Kilikoglou, V., Vekinis, G. (2001): Strength, toughness and thermal shock resistance of ancient ceramics, and their influence on technological choice. *Archaeometry*, **43**, 301–324.

Trindade, M., Dias, M., Coroado, J., Rocha, F. (2009): Mineralogical transformations of calcareous rich clays with firing: a comparative study between calcite and dolomite rich clays from Algarve, Portugal. *Appl. Clay Sci.*, **42**, 345–355.

UNE-EN 1925 (2000): Natural stone test methods. Determination of water absorption coefficient by capillarity. AENOR, Madrid, Spain.

UNE-EN 13755 (2008): Natural Stone Test Methods. Determination of Water Absorption at Atmospheric Pressure. AENOR, Madrid, Spain.

UNE-EN 15886 (2011): Conservation of Cultural Property. Test methods. Colour Measurement of Surfaces. AENOR, Madrid, Spain.

Vera, J.A. (2004): Geología de España. SGE-IGME, Madrid, Spain.

Warren, J. (1999): Conservation of Brick. Butterworth-Heinemann Series in Conservation and Museology, Butterworth Heinemann, Oxford and Boston, UK.

Whitney, D.L. & Evans, B.W. (2010): Abbreviations for names of rock-forming minerals. *Am. Mineral.*, **95**, 185–187.

Zhang, L. (2013): Production of bricks from waste materials – a review. *Constr. Build. Mater.*, **47**, 643–655.

Received 2 March 2018
Modified version received 22 October 2018
Accepted 22 October 2018